

Crystal Structures of Two Potent Nonamidine Inhibitors Bound to Factor Xa^{†,‡}

Marc Adler, Monica J. Kochanny, Bin Ye, Galina Rumennik, David R. Light, Sara Biancalana, and Marc Whitlow*

Berlex Biosciences, 2600 Hilltop Drive, P.O. Box 4099, Richmond, California 94804-0099

Received July 3, 2002; Revised Manuscript Received October 9, 2002

ABSTRACT: There has been intense interest in the development of factor Xa inhibitors for the treatment of thrombotic diseases. Our laboratory has developed a series of novel non-amidine inhibitors of factor Xa. This paper presents two crystal structures of compounds from this series bound to factor Xa. The first structure is derived from the complex formed between factor Xa and compound **1**. Compound **1** was the first non-amidine factor Xa inhibitor from our lab that had measurable potency in an in vitro assay of anticoagulant activity. The second compound, **2**, has a molar affinity for factor Xa (K_{iapp}) of 7 pM and good bioavailability. The two inhibitors bind in an L-shaped conformation with a chloroaromatic ring buried deeply in the S1 pocket. The opposite end of these compounds contains a basic substituent that extends into the S4 binding site. A chlorinated phenyl ring bridges the substituents in the S1 and S4 pockets via amide linkers. The overall conformation is similar to the previously published structures for amidine-based inhibitors complexed with factor Xa. However, there are significant differences in the interactions between the inhibitor and the protein at the atomic level. Most notably, there is no group that forms a salt bridge with the carboxylic acid at the base of the S1 pocket (Asp189). Each inhibitor forms only one well-defined hydrogen bond to the protein. There are no direct charge–charge interactions. The results indicate that electrostatic interactions play a secondary role in the binding of these potent inhibitors.

There is still an unmet need for therapeutics that can safely intervene in the thrombotic pathway. Considerable interest has been focused on factor Xa inhibitors. Factor Xa lies at the juncture of the intrinsic and extrinsic branches of the blood coagulation cascade. The factor X zymogen is activated by the factor VIIa–tissue factor complex in the extrinsic branch and by the factor IXa–factor VIIIa complex in the intrinsic branch. Factor Xa is a trypsin-like serine protease that is the catalytic member of the prothrombinase complex. The prothrombinase complex is formed from factors Va and Xa in the presence of calcium and a phospholipid membrane. This complex performs the critical step of cleaving the peptide bond of Arg302 of prothrombin, thus creating meizothrombin. Meizothrombin may be further processed into thrombin. Both thrombin and meizothrombin convert fibrinogen to fibrin and are potent activators of platelets. Experimental work with protein (1) and small molecule (2) inhibitors of factor Xa has demonstrated the efficacy of these agents as in vivo anticoagulants. These studies also suggest that factor Xa inhibitors may offer a greater degree of bleeding safety than currently available therapeutics.

An orally available factor Xa inhibitor should be useful in the treatment of chronic thrombotic diseases. Initially, our

development efforts focused on amidine-based compounds (3, 4). Crystal structures of factor Xa–inhibitor complexes have shown that the arylamidines form a salt bridge with Asp189 at the bottom of the S1 pocket (5–9). This electrostatic interaction contributes significantly to the potency of these compounds. However, the amidine group is highly basic and may contribute to the poor oral availability of these inhibitors.

A breakthrough came when our high-capacity screening group identified a novel non-amidine inhibitor of factor Xa (10). Discovery of that compound led to a series of potent and selective benzothiophene-substituted anthranilamide inhibitors (11–13). These non-amidine inhibitors retain nanomolar affinity for factor Xa even though they do not contain any positively charged atoms at neutral pH. However, the initial lead had poor physicochemical properties. Efforts to improve the potency and water solubility resulted in the discovery of compound **1**¹ (Figure 1A, K_{iapp} = 1 nM). This

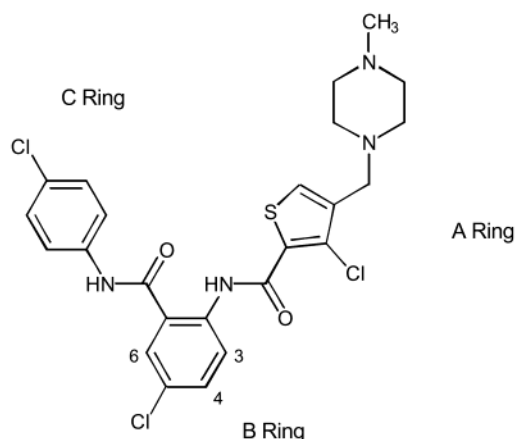
[†] The X-ray diffraction data was collected at the Stanford Synchrotron Radiation Laboratory, which is funded by the Department of Energy (BES and BER) and the National Institutes of Health (NCRR and NIGMS).

[‡] The atomic coordinates described in this paper have been deposited with the Protein Data Bank (entries 1MQ5 and 1MQ6).

* To whom correspondence should be addressed. E-mail: marc_whitlow@berlex.com. Fax: (510) 262-7844. Telephone: (510) 669-4575.

¹ Abbreviations: **1**, 3-chloro-*N*-(4-chloro-2-[(4-chlorophenyl)amino]carbonyl)phenyl)-4-[(4-methyl-1-piperazinyl)methyl]-2-thiophenecarboxamide; **2**, 3-chloro-*N*-(4-chloro-2-[(5-chloro-2-pyridinyl)amino]carbonyl)-6-methoxyphenyl)-4-[(4,5-dihydro-2-oxazolyl)methylamino]-methyl]-2-thiophenecarboxamide; EGF, epidermal growth factor; des-GLA-factor Xa β , factor Xa construct with the EGF 1 and 2 domains, and the serine protease domain; des-GLA-EGF1-factor Xa β , factor Xa construct with the EGF 2 domain and the serine protease domain; PEG, polyethylene glycol; rmsd, root-mean-square deviation; rTAP, recombinant tick anticoagulant protein; SSRL, Stanford Synchrotron Radiation Source; Tris, tris(hydroxymethyl)aminomethane; ZK-807834, *N*-(2-{5-[amino(imino)methyl]-2-hydroxyphenoxy}-3,5-difluoro-6-[3-(4,5-dihydro-1-methyl-1*H*-imidazol-2-yl)-phenoxy]pyridin-4-yl)-*N*-methylglycine; (Z,Z)-BABCH, 2,7-bis(aminobenzylidene)cycloheptan-1-one).

A) Compound 1



B) Compound 2

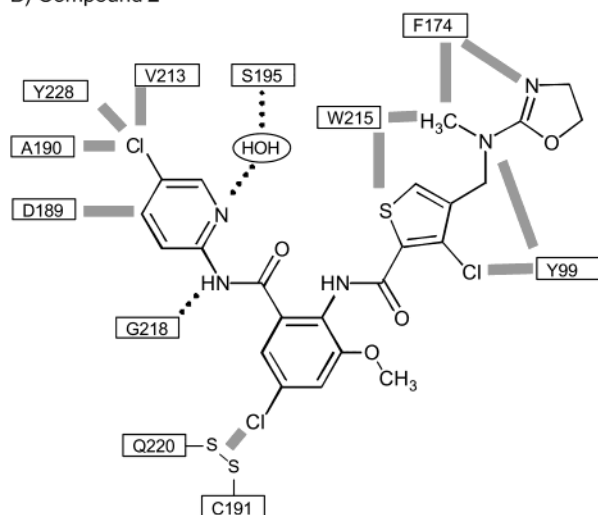


FIGURE 1: Covalent structures of compounds **1** (A) and **2** (B). Panel A shows the nomenclature for the rings and a partial numbering of the B ring. Panel B shows the major contacts between the inhibitor and factor Xa. Dotted lines represent hydrogen bonds, and thick gray lines represent contacts.

was the first compound in this series to exhibit anticoagulant activity *in vitro* using the prothrombinase assay (compound **31** in ref 12). Further optimization led to the inhibitor **2** (Figure 1B), an oxazoline-substituted derivative that has an affinity for factor Xa (K_{iapp} of 7 pM). This compound has demonstrated *in vivo* bioavailability in dogs (40%, compound **4a** in ref 13) and retains excellent selectivity against homologous serine proteases [K_{iapp} = 90 nM for human thrombin and K_{iapp} > 5000 nM for bovine trypsin (13)]. This paper presents the crystal structures of compounds **1** and **2** bound to factor Xa. These structures provide important insight into the design of non-amidine inhibitors of factor Xa and other homologous serine proteases.

EXPERIMENTAL PROCEDURES

Compound Synthesis. The synthesis and structure–activity relationships of 3-chloro-*N*-(4-chloro-2-[(4-chlorophenyl)amino]carbonyl]phenyl)-4-[(4-methyl-1-piperazinyl)methyl]-2-thiophenecarboxamide (**1**) and 3-chloro-*N*-(4-chloro-2-

[(5-chloro-2-pyridinyl)amino]carbonyl]-6-methoxyphenyl)-4-[(4,5-dihydro-2-oxazolyl)methylamino]methyl]-2-thiophenecarboxamide (**2**) and related compounds are described elsewhere (12, 13).

Preparation of Crystals. Crystals of des-GLA-EGF1-factor Xa β were grown using protocols described in our previous publication (8). Briefly, des-GLA-EGF1-factor Xa β was prepared by limited chymotrypsin (Boehringer Mannheim, Mannheim, Germany) digestion of human factor Xa β (Enzyme Research Laboratory, South Bend, IN) and purified using a MonoQ HR 5/5 anion exchange column (Amersham Pharmacia Biotech, Piscataway, NJ). Fractions B1 and B2 from anion exchange purification (Figure 1; 8) were used for crystallization. A 3-fold excess of a proprietary factor Xa inhibitor with picomolar affinity was added to des-GLA-factor Xa β . This inhibitor is based on the same template as compound **2**. The protein was then concentrated to 12–17 mg/mL. Crystals were grown using 2 μ L of complex with 2 μ L of reservoir containing 15–21% PEG1500 and 10 mM CaCl₂. Crystals took from 2 weeks to several months to form. The rate-limiting step was the slow autohydrolysis of the first EGF domain, the loss of which is required for crystal formation (8). The cell dimensions of these crystals were as follows: a = 56 Å, b = 72 Å, and c = 79 Å; the space group was $P2_12_12_1$ (crystal form 1).

The proprietary inhibitor in crystal form 1 was then displaced by either **1** or **2** using the following protocols. First, the saturation concentration of each inhibitor was determined in the crystal soaking solution [21% PEG1500, 25–50 mM Tris (pH 7.5), 20–50 mM NaCl, and 5 mM CaCl₂]. Sitting drops (30–40 μ L) containing saturated inhibitor (0.3 mM for **1** or 5 mM for **2**) in the crystal soaking solution were equilibrated over a 1 mL reservoir containing the crystal soaking solution for 1–2 days. A single factor Xa β crystal was transferred using a mounted cryoloop (Hampton Research, Liguna Niguel, CA) into one of these sitting drops and allowed to soak for ≥ 3 days. After the initial soak, each crystal was then transferred to an unused drop and allowed to soak for a second period of ≥ 3 days. This method was only successful for inhibitors that had a minimum solubility of 0.1 mM in the crystal soaking solution. The initial lead identified by the screening group (10) had poor solubility, and the inhibitor did not soak into the active site of the crystals.

A second crystal form, crystal form 2, was generated using conditions developed by Kamata et al. (6) [24% PEG3350, 0.1 M imidazole/malate (pH 5.5), 0.5 M sodium acetate (pH 5.0), and 5 mM CaCl₂]. The crystals were grown using the same proprietary inhibitor that was used for crystal form 1. These crystals have similar cell dimensions (a = 51.6 Å, b = 73.1 Å, and c = 81.4 Å) and share the same space group ($P2_12_12_1$) as the crystals described above.

Crystallographic Data Collection. A crystal was transferred from its crystallization drop to a drop containing 15% glycerol, 7.5% (*R,R*)-(-)-2,3-butanediol (Sigma, St. Louis, MO), 15.75% PEG1500 (Hampton Research), and 7.5 mM CaCl₂ for approximately 30 s, prior to being flash-frozen at 100 K in the Stanford Synchrotron Radiation Source (SSRL) beamline cryostream. The diffraction data from a factor Xa β –**1** crystal were collected on SSRL beamline 7-1. Ninety-two images were collected using a 1.0° sweep per frame, a 100 s exposure, and a detector distance of 220 mm.

Table 1: X-ray Diffraction Data and Refinement Statistics

	1	2
space group	$P2_12_12_1$	$P2_12_12_1$
wavelength (Å)	1.080	1.033
unit cell dimensions (Å)		
<i>a</i>	56.36	56.64
<i>b</i>	72.02	72.29
<i>c</i>	78.92	79.02
no. of reflections	18977	19603
resolution range (Å)		
high	2.10 (2.10) ^a	2.10 (2.10) ^a
low	~25 (2.19)	~25 (2.19)
completeness (%)	98.2 (97.5)	99.1 (98.4)
redundancy	3.6 (3.7)	3.5 (3.7)
R_{sym}^b	0.054 (0.338)	0.067 (0.361)
mean $I/\sigma(I)$	12.0 (2.2)	8 (1.3) ^c
refinement		
resolution (Å)	8.0–2.10	8.0–2.10
no. of reflections		
input	18602	17183
used ($F > 2\sigma$)	18308	15521
<i>R</i>	0.190 (0.284)	0.186 (0.293)
R_{free}	0.264 (0.343)	0.268 (0.337)
no. of solvent molecules	172	164
no. of glycerol molecules + 1Ca ²⁺	3	3
rms deviation for ideal	0.011	0.011
bond lengths (Å)		
rms deviation for ideal	2.02	2.01
bond angles (deg)		

^a Statistics for the highest-resolution shell of data are shown in parentheses. ^b $R_{\text{sym}} = \sum |I - \langle I \rangle| / \sum I$. ^c For this data set, mean $I/\sigma(I) = 2.0$ at 2.26 Å.

Images were recorded using the 300 mm plate on a Mar345 detector (Mar Research, Norderstedt, Germany). The images were processed with Mosflm and Scala using the SSRL scripts (14, 15). The diffraction data from a factor Xaβ–2 complex crystal were collected on SSRL beamline 9-2. Three hundred sixty-eight deindexed images were collected using 30 s exposure times, a 0.25° sweep per image, and a detector distance of 150 mm. Images were recorded by a Quantum-4 detector (Area Detector Systems Corp., San Diego, CA). After subtraction of the 14 counts from each image to reduce the pedestal value to six counts, the images were processed with X-GEN (16, 17) from Accelrys Inc. (San Diego, CA). Both crystals were in space group $P2_12_12_1$ (Table 1).

Crystallographic Structure Determination and Refinement. The data were processed using the same techniques outlined in our previous publication (8). The initial model was based on the published structure of the factor Xa–ZK-807834 complex [1FJS (8)]. All heteroatoms except the calcium were stripped from the coordinates. This model was fit to the data using rigid body refinement (18) using data from 8.0 to 3.0 Å. Simulated annealing (18) was then used to refine the structure as the higher-resolution data were introduced into successive steps. The inhibitors were fit to the data once the resolution had been extended to 2.3 Å. Waters were added to the structures (19) in all subsequent steps. The programs X-plor 3.1 (18), O (20), and Xtalview (19) were used in the refinement of the data from 8.00 to 2.10 Å. The residues are numbered using the chymotrypsin numbering system of Padmanabhan et al. (21).

Preparation of Figures. Figures 3, 5, and 6 were prepared with ViewerPro 4.2. Figure 2 was prepared with XtalView using the blob option with minor editing of the postscript

files. Figure 4 was prepared with insightII. All software was provided by Accelrys.

RESULTS

Crystal Growth and Characterization. During the course of the project, crystals were grown using two different protocols that yielded two distinct crystal forms. In both cases, we used a picomolar inhibitor of factor Xa in the initial crystallization. The inhibitor is based on the same thiophene template as compound 2. This inhibitor was selected because it gave reproducible results. The picomolar inhibitor was then displaced from the crystal by soaking it in a solution of either compound 1 or 2.

The X-ray structures presented here were obtained from crystals grown using our previously published techniques (8). The space group was $P2_12_12_1$ with the following unit cells: $a = 56.36$ Å, $b = 72.02$ Å, and $c = 78.92$ Å for 1, and $a = 56.64$ Å, $b = 73.29$ Å, and $c = 79.02$ Å for 2 (Table 1). These crystals were isomorphous to those used by several investigators (6–9) and are termed crystal form 1.

The electron density from both crystals (Figure 2) indicates that there was complete exchange between these inhibitors and the inhibitor used in the initial crystallization. The initial inhibitor has a different A ring substituent in the S4 pocket. There are at least two heavy atoms in this ring that are clearly resolved from the S4 groups of compounds 1 and 2. These atoms lie outside the 0.6σ level of the electron density in both structures.

A second set of crystals were grown using the conditions described by Kamata et al. (6). These conditions produced new crystals (crystal form 2) that are distinct from the ones described above as well as the crystal form observed by the original authors (6). The unit cell dimensions are as follows: $a = 51.6$ Å, $b = 73.1$ Å, and $c = 81.4$ Å; the space group is $P2_12_12_1$. Notably, the *A* axis of this new form is 5 Å shorter in length than that in crystal form 1. The structure was solved for crystal form 2 using the program AMORE (22) to perform molecular replacement. The starting model was the factor Xa coordinates from PDB entry 1FJS (8). Unlike crystal form 1, the picomolar inhibitor appears at the crystal packing interface. The thiophene ring is in close contact (4.0 Å) with Cα and Cβ atoms of Asn120 from the EGF1 domain from a symmetry-related molecule. Formation of this alternate crystal form is, doubtless, dependent on the properties of the inhibitor. Experience has shown that the inhibitor is trapped in crystal form 2 and cannot be displaced by soaking. The original conditions of Adler et al. (8) were used in all subsequent experiments.

Structures. The crystal structures of compounds 1 and 2 complexed to factor Xa were refined to 2.10 Å (Table 1; PDB entries 1MQ5 and 1MQ6). The values of *R* and R_{free} for the 2 complex were 18.7 and 26.8%, respectively. The corresponding values for the 1 complex were 19.0 and 26.4%, respectively. The final model of the factor Xa–2 complex contains residues 87–137 of the light chain, residues 16–243 of the heavy chain (catalytic domain), compound 2, one calcium ion, three molecules of glycerol, and 164 waters. The factor Xa–1 model is built from the same constituents and differs only in the inhibitor and that it uses a total of 172 waters. Figure 2 shows the electron density for 1 and 2 bound to factor Xa. Compound 2 is completely contained

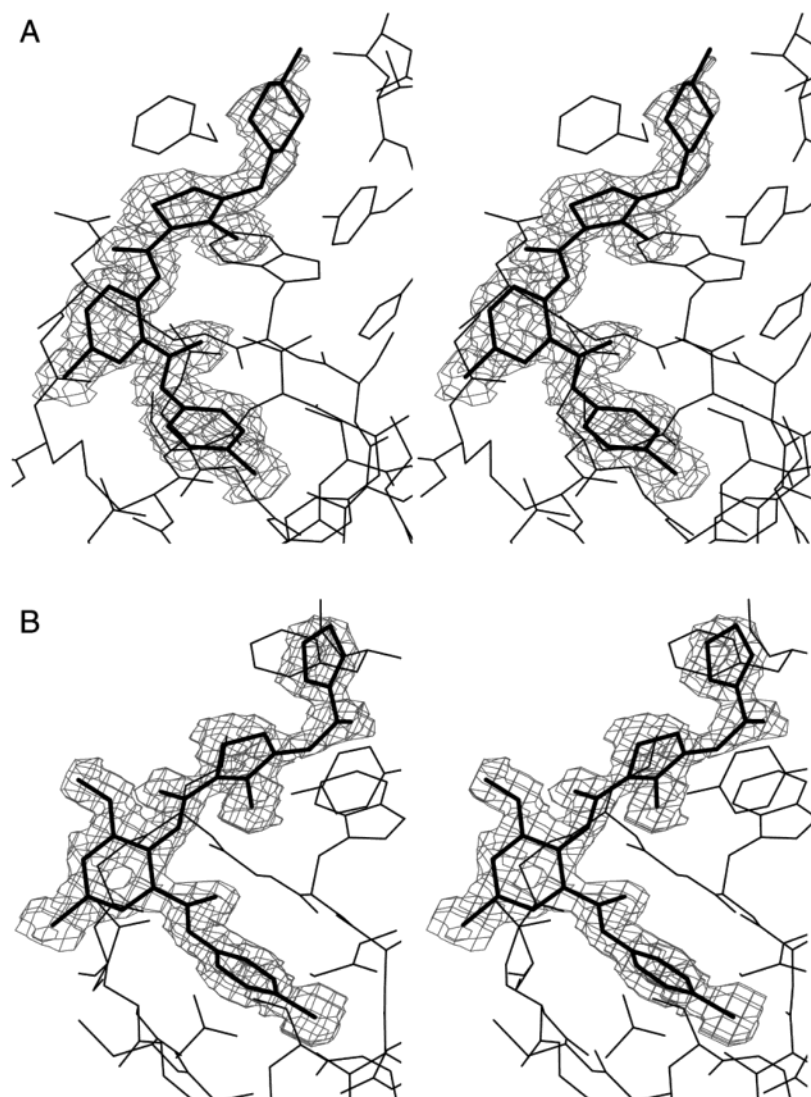


FIGURE 2: (A) Divergent stereoview of the electron density around compound **1** in factor Xa. The $2F_o - F_c$ electron density map is displayed at 1.0σ and is shown with gray lines, and the inhibitor is shown with thick lines. (B) Electron density around compound **2** in factor Xa. The shading is the same as in panel A.

within the 1σ contour of the $2F_o - F_c$ map. With the exception of the piperazine ring, compound **1** is also enclosed in the 1σ map.

Both inhibitors bind in the classic L-shaped configuration (Figures 2 and 3) that has been seen in the structures of amidine-based inhibitors of factor Xa (5–9). The two arms of the inhibitors (C ring and A ring, Figure 1) extend into the S1 and S4 pockets (Figure 4). The six-membered B ring connects to the two arms through amide linkers. Figure 1B shows the major contacts between compound **2** and the protein. For **2**, the relative positions of the oxygen and nitrogen atoms in the oxazoline ring cannot be determined from the X-ray data and the orientation of the ring is arbitrary.

Our initial discussion focuses on the more potent of the two inhibitors, compound **2**. Overall, the bound conformation of **2** (Figure 5A) is similar to the corresponding structure for our benzamidine-based inhibitor ZK-807834 [PDB entry 1FJS (8)]. However, there are major differences in the interactions with factor Xa at the atomic level. These differences are most pronounced in the S1 pocket. The S1

site is believed to bind Arg302 of prothrombin, the natural substrate of factor Xa. The chloropyridine ring of **2** (ring C, Figure 1) replaces the benzamidine group of ZK-807834 in the S1 pocket (Figure 5A). Compound **2** does not have a charged group that forms a salt bridge with the carboxyl group of Asp189. The carbon in position 4 (C5) of ring C has the closest contact with this acidic group (3.5 \AA). The chlorine on the C ring makes contacts with the backbone oxygen of Ile227 (3.8 \AA) and the phenol hydroxyl of Tyr228 (3.5 \AA). This chlorine also has hydrophobic contacts with $C\gamma_1$ of Val213 (3.7 \AA), the phenol ring of Tyr228 (3.4 \AA), and $C\beta$ of Ala190 (3.7 \AA). A similar conformation for chloroaromatic groups has been observed in the S1 pocket of thrombin (23), trypsin (24), and urokinase (25, 26).

The nitrogen in the pyridine ring forms a water-mediated hydrogen bond to the active site serine (Ser195). The substitution of pyridine for phenyl in ring C results in a 2–15-fold improvement in binding affinity (ref 13 and unpublished data). This indicates that the strength of the hydrogen bond can vary with minor changes in the template. The close contact between the pyridine nitrogen

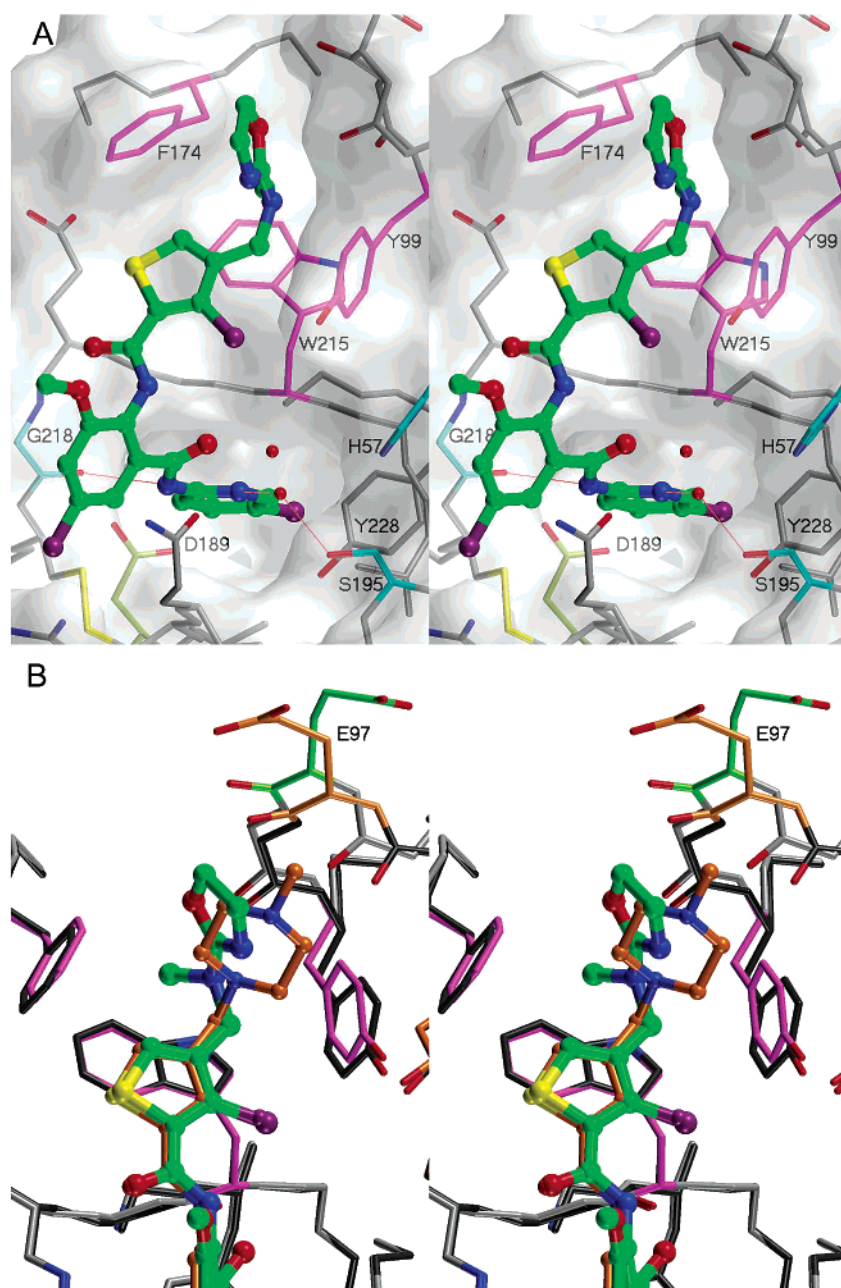


FIGURE 3: (A) Divergent stereoview of the bound conformation of **2**. Carbon atoms of specific residues have been colored. Compound **2** is colored in green, and its chlorine atoms are purple. Residues that form the S4 pocket (Tyr99, Phe174, and Trp215) are magenta. Asp189 at the bottom of the S1 pocket is light green. Gly218 is light blue. Two residues from the catalytic triad (Ser195 and His57) are cyan. The hydrogen bonds are depicted as red lines. The solvent accessible surface of the protein is depicted as a translucent gray shell. A few residues (59–61 and 192) were not included in this surface to improve the visibility of the active site cleft. (B) Detailed view into the S4 pocket for both compounds **1** and **2**. The carbon atoms are green for compound **2** and gold for **1**. For the protein itself, the backbone and carbon atoms in the factor Xa–**2** structure are gray and the corresponding ones in the **1** complex are black. Glu97 has been labeled in light green for **2** and gold in **1**.

and water 736 (3.0 Å) provides enough information to orient the pyridine ring in this structure. No corresponding water was found in contact with the C ring phenyl of compound **1**.

The central phenyl ring (B ring) of compound **2** forms a bridge between the substituents in the S1 and S4 pockets through amide bonds. There is a hydrogen bond between the amide nitrogen of the B–C linker and the carbonyl of Gly218 (3.0 Å). There is also a second long hydrogen bond between the nitrogen of Gly218 and the carbonyl oxygen of the A–B linker (3.4 Å). Figure 5A shows that the B ring of

2 is shifted by 3 Å from the comparable pyridine ring of ZK-807834. This shift affects the position of the B–C linker and increases the distance between the amide nitrogen and the active site Ser195 O γ (6.3 Å), thus protecting the amide from cleavage. The 5-chloro substituent on the B ring extends into a small pocket (Figure 4) and makes contact with the disulfide bridge between Cys191 and Cys220 (3.7 Å). This site has been previously called the S1 β pocket in a structure of human urokinase (27). The 3-methoxy substituent is solvent-exposed, which indicates that substitutions at this position will have only minor effects on potency.

The binding interactions in the S4 pocket (Figure 5A) for compound **2** and ZK-807834 are surprisingly similar considering their divergent structures. The thiophene ring of **2** (A ring) stacks against the side chain of Trp215 (3.7 Å) and occupies the same site as the phenoxy linker in ZK-807834 (Figure 5A). The oxazoline ring is squeezed between the side chains of Tyr99 (3.9 Å) and Phe174 (3.4 Å), which is where the 1-methyl-2(1*H*)-imidazoline group of ZK-807834 is located (Figure 5A). Both **2** and ZK-807834 have a methyl group in the proximity of the indole of Trp215 (<3.5 Å).

Crystal Structure of Compound 1. Both compounds **1** and **2** bind in the same conformation to factor Xa (Figure 3B) even though there is a 100-fold difference in potency. The root-mean-square deviation (rmsd) of the atom coordinates for the A–C rings of these inhibitors is 0.20 Å. By comparison, the rmsd of the C α atoms of the catalytic subunit of the associated protein is 0.25 Å. Recent work (13) has demonstrated that the bulk of the difference in the binding affinity of these compounds can be ascribed to the substituents on the thiophene ring (A ring). There are two other substitutions that had smaller effects on potency. The phenyl C ring of **1** has been changed to a pyridine in **2**, and the 3-methoxy group has been added to the B ring in **2**. Combined, these two modifications yield a 5-fold increase in activity (13; Table 1).

Figure 3B shows in detail the interaction in the S4 pocket of both compounds. The loop containing residues 96–98 has three backbone carbonyls and one acidic side chain (Glu97) that can interact with the positively charged thiophene substituent. However, for the more potent inhibitor, **2**, the backbone of this loop is 0.7 Å further away from the charged ring. For the less potent inhibitor, **1**, the backbone carbonyl of Glu97 comes in close contact with the piperazine ring (2.8 Å). The corresponding contact distance in **2** measures 3.4 Å. Furthermore, the acidic side chain of Glu97 points toward **1** (4.4 Å) and away from **2** (7.5 Å). The results suggest that the interactions with the electronegative groups in the S4 pocket do not correlate with the potency of the inhibitors in this series. The interactions with the aromatic rings of Tyr99, Phe174, and Trp215 may make the most important contributions to the binding interactions in the S4 pocket.

DISCUSSION

Compound **2** is the most potent (7 pM) inhibitor of factor Xa for which a crystal structure has been published. **2** represents an optimization of a lead that was identified by high-capacity screening (10). The structure–activity relationships point out two key contributions for the increases in potency for compounds in this series: the 4-chloro substitution in the S1 pocket and the methylaminooxazoline in the S4 pocket. Substitutions on the central B ring had smaller effects on affinity (ref 11 and unpublished data).

Structure–Activity Relationship within the Thiophene Series. The interactions in the S1 pocket are critical for factor Xa inhibitors. Our best results have come from compounds such as **2** that have a single aromatic ring substituted with either chlorine or bromine para to the attachment point (11). Figure 3A shows that this halogen is in close contact (<3.8 Å) with four residues at the base of the S1 pocket. Other

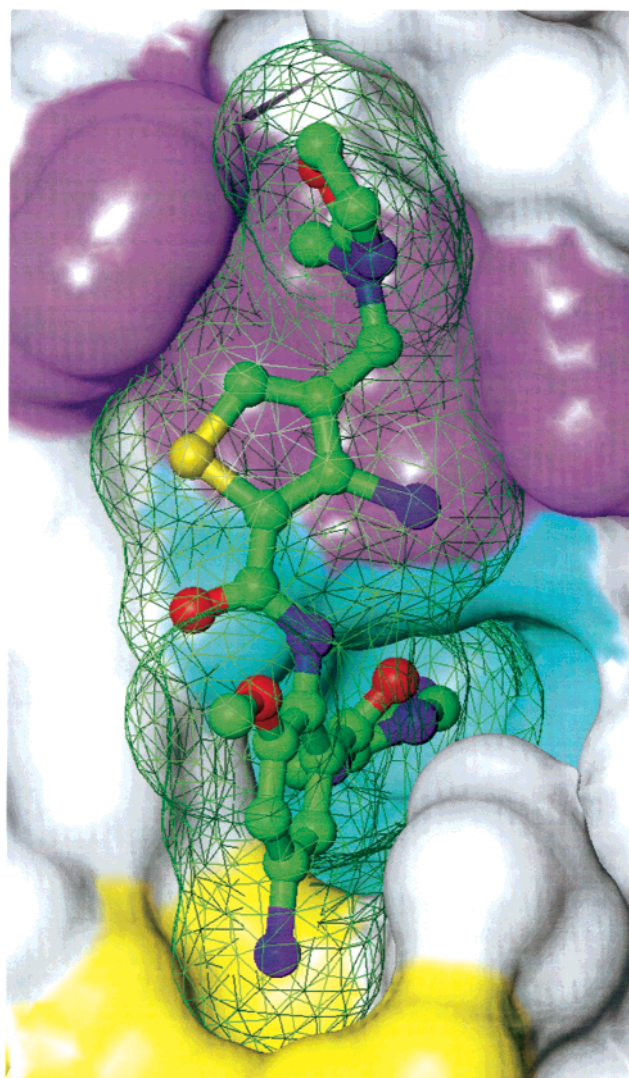
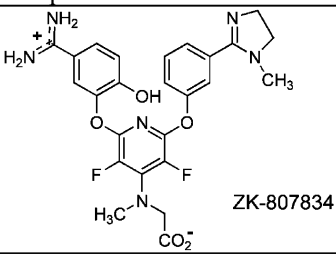
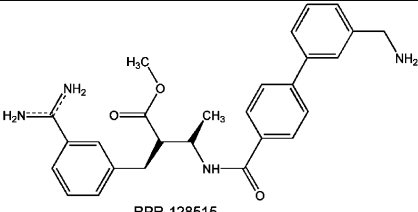
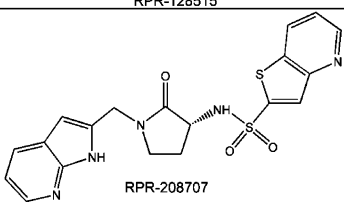
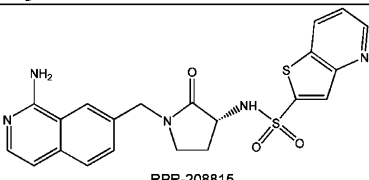


FIGURE 4: Connelly surfaces of compound **2** bound to factor Xa. The surface of the inhibitor is shown as a green wire cage. The protein surface is solid and is colored as follows: S1 β is yellow, S1 light blue, and the hydrophobic part of S4 magenta. The rest of the protein is white.

substitutions cause a significant reduction in potency (>20-fold). Examples include F, H, CH₃, OCH₃, COOH, and NH₂ (11; Table 1). It appears that neither size (OCH₃) nor partial negative charge (F) is sufficient for tight binding. It is possible that there is some interaction between the larger halogens and the aromatic ring of Tyr228 (3.4 Å).

The chlorine on the C ring also plays an important role in the selectivity of this template against trypsin [$K_{iapp} > 5000$ nM for bovine trypsin (13)]. The chlorine is in close contact with C β of Ala190 (3.7 Å). In trypsin, there is Ala to Ser substitution at this position. A recent X-ray structure [1QL7 (24)] of a factor Xa inhibitor bound to bovine trypsin indicates that there would be a steric clash between the chlorine of our inhibitors and Ser190 O γ . In 1QL7, the factor Xa inhibitor has a chlorinated naphthyl ring that binds in roughly the same position as the S1 substituent of compounds **1** and **2**. The 1QL7 structure indicates that the chlorine forces Ser190 O γ out of the S1 pocket. This steric clash may explain why these compounds have reduced affinity for trypsin.

Table 2: Factor Xa Inhibitor Complexes^a

Compound	K _i (nM)	PDB Entry	Reference
 ZK-807834	0.2	1FJS	8
 RPR-128515	0.9	1EZQ	7
 RPR-208707	18	1FOS	7
 RPR-208815	22	1FOR	7

^a For the sake of brevity, the following amidine-based inhibitors were omitted from the table: DX-9065a, K_i = 41 nM [1FAX (5)]; FX-2212a, K_i = 272 nM [1XKA (6)]; BIBT0871, K_i = 57 nM [1G2L (9)]; and BIBT1109, K_i = 40 nM [1G2M (9)].

The central B ring of **2** has only minimal contacts with the protein through the C5 and C6 sites. C6 is close to S_γ of Cys220 (3.5 Å), and substitutions at the position abolished activity (11; Table 3). The 5-chloro substituent fills the small S1_β pocket (Figure 4) and improves the potency by 10-fold. Substitutions on C5 are the only ones on the B ring that significantly increase binding affinity (11). Both the C3 and C4 positions of the central anthranilic acid ring are solvent-exposed. Substituents at the C4 position have a limited effect on the factor Xa potency. The C3 methoxy is in close contact with the amide carbonyl (3.0 Å) from the A–B linker, and alternate substitutions at C3 may introduce unfavorable steric interactions.

There has been an extensive synthetic work performed on the A ring substituent for this thiophene template (11–13). The A ring in **2** fills the S4 binding pocket of factor Xa (Figure 4). The best results have been obtained from inhibitors with a hydrophilic group attached by at least one rotatable bond to the thiophene ring. The X-ray structures of compounds **1** and **2** show that there is fair amount of conformational flexibility in the residues lining the S4 pocket.

Compound **1** has an *N*-Me-piperazine in place of the methylaminooxazoline of compound **2** (Figure 1). Previous measurements have shown most of the 100-fold loss of potency in **1** can be ascribed to changes in the substituent attached to the A ring (13). The piperazine of **1** is unsaturated. Unlike the oxazoline ring, the piperazine cannot

participate in any aromatic ring stacking with Tyr99 and Phe174. Furthermore, the piperazine of **1** lacks the *N*-methyl that can interact with the ring system of Trp215. The methyl substituent attached to the oxazoline ring of **2** maintains close contact with the indole of Trp215 (3.5 Å). This interaction has been observed in our most potent factor Xa inhibitors.

Several investigators, including ourselves (5, 8, 28), have speculated that electronegative groups from residues 96–98 help to counterbalance the positive charge in the S4 pocket. However, there is little correlation between the interaction with residues 96–98 and the potency of the inhibitors (refs 7 and 8 and the work presented here). Furthermore, there are several compounds based on this thiophene template that have neutral substituents attached to the thiophene ring and retain sub-nanomolar potency (13). The basic group was added to the thiophene template to improve the water solubility of these compounds (12). There were only minor effects on the potency of the inhibitors.

Comparison between Factor Xa Inhibitors. The Protein Data Bank now contains 10 structures of synthetic inhibitors bound to factor Xa (Table 2, refs 5–9, and data presented here). These inhibitors can be divided into two classes based on their potency: high-affinity inhibitors (<1 nM) (1MQ5, 1MQ6, 1FJS, and 1EZQ) and low-affinity inhibitors (>10 nM) (1F0S, 1F0R, 1FAX, 1XKA, 1G2L, and 1G2M). All of these compounds have at least one aromatic ring in the S1 pocket and a basic group in the S4 site.

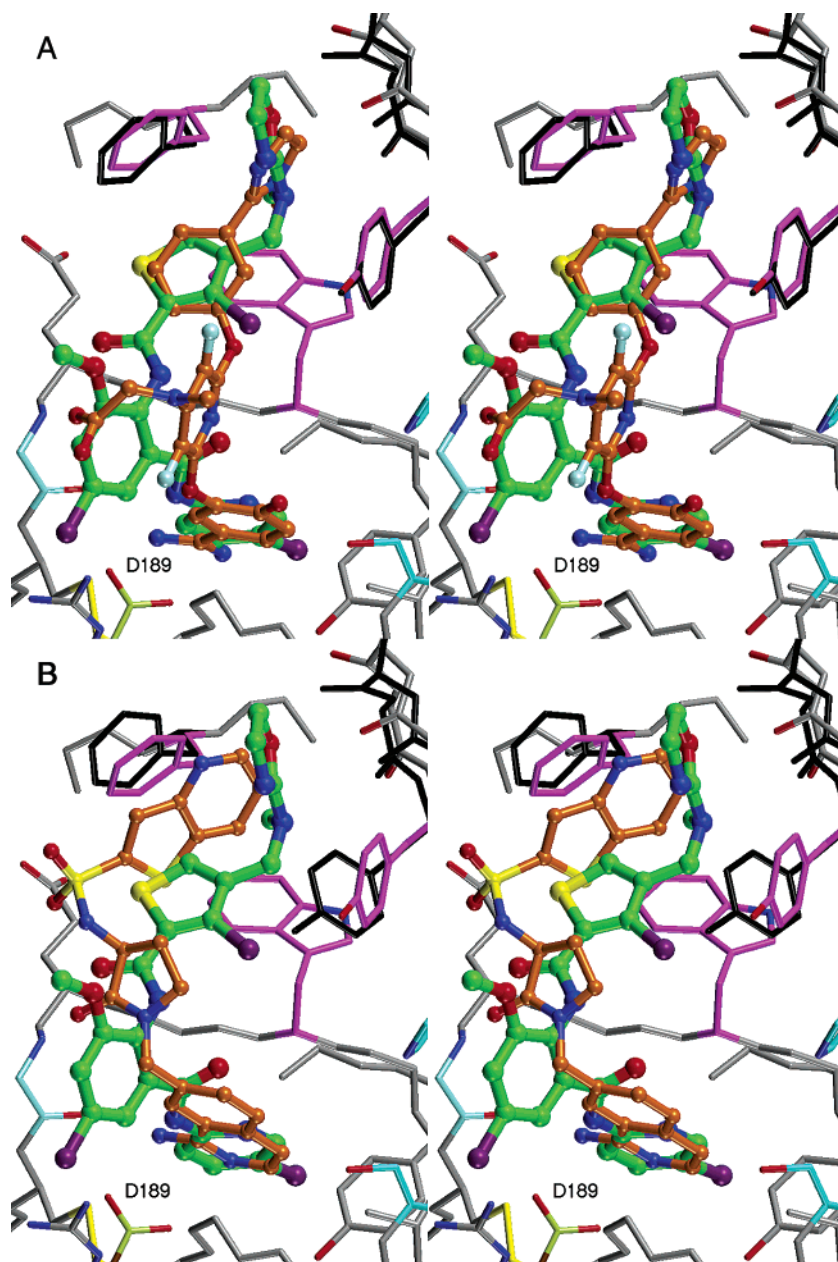


FIGURE 5: (A) Divergent stereoview of the superposition of the structures of compound **2** and ZK-807834. The color scheme is the same as in Figure 3A. The carbon atoms of ZK-807834 are gold. A limited number of protein atoms in the S4 pocket of the ZK-807834 complex are black. The side chain of Gln192 has been omitted to improve the view into the S1 pocket. (B) Superposition of the structures of compound **2** and RPR208815. The coloring is the same as in panel A.

The high-affinity inhibitors all have a single aromatic ring in the S1 pocket with either an amidine in the meta position [1FJS (8) and 1EZQ (7)] or a chlorine in the para position (1MQ5 and 1MQ6). Both types of inhibitors extend to the base of the S1 pocket and make contact with Asp189 (<3.6 Å) through either the amidine group (1FJS and 1EZQ) or a chlorinated aromatic ring (1MQ5 and 1MQ6). These interactions in the S1 pocket seem to be essential for the potency for factor Xa inhibitors that directly block the active site.

The two related non-amidine inhibitors from Aventis, RPR208707 [1F0R (7)] and RPR208815 [1F0S (7)], have either a 7-azaindole or a 1-aminoisoquinoline ring system in the S1 pocket (Table 2). The crystal structures reveal a surprisingly large gap at the base of the S1 pocket (Figure 5B). In both structures, there is a water-mediated hydrogen

bond between a ring nitrogen and Asp189. Comparisons to a meta-substituted benzamidine from the same series [RPR131247 (7)] indicate that there is a 30-fold loss of affinity for the amidine replacement, which suggests that further optimization is possible.

A comparison between the factor Xa inhibitors shows that there is a wide variation in the linkers that connect the substituents in the S1 and S4 binding sites.² There is little conservation for either the interactions with the protein or the covalent structure of the linkers. Three of the linkers are

² Compounds **1** and **2** are based on the same template and have nearly identical linkers. The discussion will focus on compound **2**. Similarly, the non-amidine inhibitors from Aventis, RPR208707 and RPR208815, differ only in the S1 substituent and bind in nearly identical fashions. For the sake of brevity, only RPR208707 (1F0R) will be discussed further.

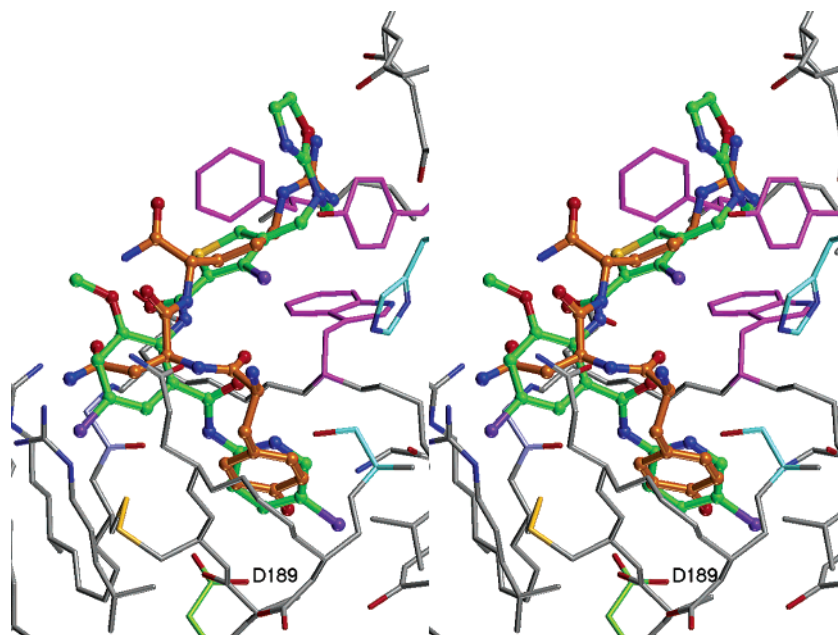


FIGURE 6: (A) Divergent stereoview of the superposition of the structures of compound **2** and the first three residues of rTAP. The color scheme is the same as that in Figure 3A. The carbon atoms of rTAP are gold.

positioned near Gly218: **2** (1MQ6), RPR128515 (1EZQ), and RPR208707 (1F0R). There is a hydrogen bond formed between the nitrogen in Gly218 and a carbonyl in each inhibitor, although in our structures this bond is extended (3.4 Å) and may not significantly contribute to the binding energy. Two of these inhibitors, **2** and RPR128515, have a small substituent in the S1 β pocket (Figure 5B). The linker in ZK-807834 (1FJS) binds in a different mode. Its only direct contact with the protein is through the side chain of Gln192. Four other amidine-based inhibitors, DX-9065a [1FAX (5)], FX-2212a [1XKA (6)], BIBT0871 [1G2L (9)], and BIBT1109 [1G2M (9)], adopt roughly the same conformation as ZK-807834, despite their markedly different chemical structures. A third orientation is seen for the linker in (Z,Z)-BABCH [2,7-bis(amidinobenzylidene)cycloheptan-1-one] (ref 29 and unpublished data). The edge of the heptanone ring contacts the active site His57 (3.7 Å). Our own design efforts have focused on limiting the conformational flexibility of these linkers. Perhaps the most important function of the linker may simply be to present the S1 and S4 substituents in their proper orientation.

In factor Xa, the S4 pocket is a narrow channel defined by the aromatic rings of Tyr99, Phe174, and Trp215 (Figures 3A and 4). The side chains of Tyr99 and Phe174 form the sides of the channel. Comparisons between structures show that residues move to accommodate inhibitors of different sizes (5–9). The rmsd of the two C ζ atoms of Tyr99 and Phe174 is 0.7 Å for the superimposed structures of the various factor Xa structures in the database. There is also a fair amount of flexibility in the loop containing residues 96–98. The rmsd of Glu97 C α is 0.5 Å, and the location of the side chain C γ varies by 2.1 Å. The Trp215 side chain, which forms the floor of the channel, is fixed by comparison (rmsd of Trp215 C ϵ_2 is 0.2 Å).

There is surprising similarity in the binding of the S4 substituent for the high-potency (<1 nM) factor Xa inhibitors: **1**, **2**, ZK-807834 (8), (Z,Z)-BABCH (29), and RPR-128515 (7). A nonpolar aromatic ring extends across the face

of Trp215. The edges of this ring are in contact with the side chains of Tyr99 and Phe174. A basic group is connected to this aromatic ring by a rotatable bond. This basic group is squeezed between Tyr99 and Phe174 (Figure 4), and it is roughly perpendicular to the nonpolar aromatic ring. With the noted exception of compound **1**, there is at least one close contact (<3.5 Å) between the basic group and the indole of Trp215.

There is one more published structure of a factor Xa inhibitor that is surprisingly similar to our non-amidine inhibitors **1** and **2**. The highly selective protein inhibitor, recombinant tick anticoagulant protein (rTAP), binds to bovine factor Xa and forms many of the same contacts as compounds **1** and **2**. Figure 6 shows a superimposition of **2** and rTAP [1KIG (30)]. Both inhibitors have an uncharged aromatic ring in the S1 pocket. Both inhibitors also have a basic group in the S4 pocket connected by a hydrophobic linker. It is surprising that our chemists have developed a non-amidine inhibitor of factor Xa that mimics a naturally occurring inhibitor.

Finally, our structure of the factor Xa–**2** complex demonstrates that potent factor Xa inhibitors do not require a basic group that binds in the S1 pocket. Compound **2** is a 7 pM inhibitor of factor Xa that only has one direct hydrogen bond. There are no salt bridges and no charge–charge interactions. Figure 4 does show that there is an excellent shape complementary between the inhibitor and the protein that includes an extremely tight fit in the S1 pocket. The structure implies that good electrostatic interactions are not required for high-potency inhibitors.

ACKNOWLEDGMENT

We thank Drs. William Dole and John Morser for the support of this work. Dr. Amy Liang determined the inhibition constants for our factor Xa inhibitors. Furthermore, we thank Dr. Gary Phillips for his insight and editorial assistance in preparing the manuscript.

REFERENCES

1. Nicolini, F. A., Lee, P., Malucky, J. L., Lefkovits, J., Kottke-Marchant, K., Plow, E. F., and Topol, E. J. (1996) Selective inhibition of factor Xa during thrombolytic therapy markedly improves coronary artery patency in a canine model of coronary thrombosis, *Blood Coagulation Fibrinolysis* 7, 39–48.
2. Abendschein, D. R., Baum, P. K., Martin, D. J., Vergona, R., Post, J., Rumennik, G., Sullivan, M. E., Eisenberg, P. R., and Light, D. R. (2000) Effects of ZK-807834, a novel inhibitor of factor Xa, on arterial and venous thrombosis in rabbits, *J. Cardiovasc. Pharmacol.* 35, 796–805.
3. Phillips, G. B., Buckman, B. O., Davey, D. D., Eagen, K. A., Guilford, W. J., Hinchman, J., Ho, E., Koovakkat, S., Liang, A., Light, D. R., Mohan, R., Ng, H. P., Post, J., Smith, D., Shaw, K. J., Subramanyam, B., Sullivan, M. E., Trinh, L., Vergona, R., Walters, J., White, K., Whitlow, M., Wu, S., Xu, W., and Morrissey, M. M. (1998) Discovery of N-[2-[5-[Amino(imino)methyl]-2-hydroxyphenoxy]-3,5-difluoro-6-[3-(4,5-dihydro-1-methyl-1H-imidazol-2-yl)phenoxy]pyridin-4-yl]-N-methylglycine (ZK-807834): a potent, selective, and orally active inhibitor of the blood coagulation enzyme factor Xa, *J. Med. Chem.* 41, 3557–3562.
4. Phillips, G., Davey, D. D., Eagen, K. A., Koovakkat, S. K., Liang, A., Ng, H. P., Pinkerton, M., Trinh, L., Whitlow, M., Beatty, A. M., and Morrissey, M. M. (1999) Design, synthesis, and activity of 2,6-diphenoxypyridine-derived factor Xa inhibitors, *J. Med. Chem.* 42, 1749–1756.
5. Brandstetter, H., Kuhne, A., Bode, W., Huber, R., von der Saal, W., Wirthensohn, K., and Engh, R. A. (1996) X-ray structure of active site-inhibited clotting factor Xa. Implications for drug design and substrate recognition, *J. Biol. Chem.* 271, 29988–29992.
6. Kamata, K., Kawamoto, H., Honma, T., Iwama, T., and Kim, S.-H. (1998) Structural basis for chemical inhibition of human blood coagulation factor Xa, *Proc. Natl. Acad. Sci. U.S.A.* 95, 6630–6635.
7. Maignan, S., Guilloteau, J. P., Pouzieux, S., et al. (2000) Crystal structures of human factor Xa complexed with potent inhibitors, *J. Med. Chem.* 43, 3226–3232.
8. Adler, M., Davey, D. D., Phillips, G. B., Kim, S.-H., Jancarik, J., Rumennik, G., Light, D. R., and Whitlow, M. (2000) Preparation, Characterization and the Crystal Structure of the Inhibitor ZK-807834 (CI-1031) Complexed with Factor Xa, *Biochemistry* 39, 12534–12542.
9. Nar, H., Bauer, M., Schmid, A., Stassen, J. M., Wienen, W., Priepke, H. W., Kauffmann, I. K., Ries, U. J., and Huel, N. H. (2001) Structural basis for inhibition promiscuity of dual specific thrombin and factor Xa blood coagulation inhibitors, *Structure* 9, 29–37.
10. Liang, A. M., Light, D. R., Kochanny, M. J., Rumennik, G., Trinh, L., Lentz, D., Post, J., Morser, J., and Snider, M. (2002) Discovery and characterization of a potent and selective non-amidine inhibitor of human factor Xa, *Biochem. Pharmacol.* (in press).
11. Chou, Y.-L., Davey, D. D., Eagan, K. A., Griedel, B. D., Karanjowala, R., Phillips, G. B., Sacchi, K. L., Shaw, K. J., Wu, S. C., Lents, D., Liang, A. M., Trinh, L., Morrissey, M. M., and Kochanny, M. J. (2002) Structure–Activity Relationships of Substituted Benzothienophene-Anthranilamide Factor Xa Inhibitors, *Bioorg. Med. Chem. Lett.* (in press).
12. Kochanny, M. J., Griedel, B. D., Wheesong, L., Karanjowala, R., Phillips, G. B., Sacchi, K. L., Sakata, S. T., Ye, B., Zhao, Z., Adler, M., Ewing, J., Lents, D., Liang, A. M., Post, J., Whitlow, M., Morrissey, M. M., and Shaw, K. J. (2002) unpublished results.
13. Bin, Y., Chou, Y.-L., Griedel, B. D., Karanjowala, R., Wheesong, L., Sacchi, K. L., Sakata, S. T., Shaw, K. J., Wu, S. C., Zuchen, Z., Cheeseman, S., Ewing, J., Fitch, R., Lentz, D., Liang, A., Post, J., Subramanyam, B., Vergona, R., Walters, J., Wang, Y.-X., White, K. A., Morrissey, M. M., and Kochanny, M. J. (2002) unpublished results.
14. Leslie, A. G. W. (1990) *Crystallographic Computing*, Oxford University Press, New York.
15. Collaborative Computational Project No. 4 (1994) *Acta Crystallogr. D* 50, 760–763.
16. Howard, A. J., Gilliland, G. L., Finzel, B. C., Poulos, T. L., Ohlendorf, D. H., and Salemme, F. R. (1987) Use of an imaging proportional counter in macromolecular crystallography, *J. Appl. Crystallogr.* 20, 383–387.
17. Accelrys Inc. X-GEN product information. <http://www.accelrys.com/ceius2/c2xgen.html> (July 1, 2002).
18. Brünger, A. (1993) *X-PLOR: A System for X-ray Crystallography and NMR*, Version 3.1, Yale University Press, New Haven, CT.
19. McGee, D. E. (1992) *J. Mol. Graphics* 10, 44–46.
20. Jones, T. A., Zou, J. Y., Cowan, S. W., and Kjeldgaard, M. (1991) Improved methods for binding protein models in electron density maps and the location of errors in these models, *Acta Crystallogr. A* 47, 110–119.
21. Padmanabhan, K., Padmanabhan, K. P., Tulinsky, A., Park, C. H., Bode, W., Huber, R., Blankenship, D. T., Cardin, A. D., and Kisiel, W. (1993) Structure of human des(1–45) factor Xa at 2.2 Å resolution, *J. Mol. Biol.* 232, 947–966.
22. Navaza, J. (1994) *Acta Crystallogr. A* 50, 157–163.
23. Tucker, T. J., Brady, S. F., Lumma, W. C., Lewis, S. D., Gardell, S. J., Naylor-Olsen, A. M., Yan, Y., Sisko, J. T., Stauffer, K. J., Lucas, B. J., Lynch, J. J., Cook, J. J., Stranieri, M. T., Holahan, M. A., Lyle, E. A., Baskin, E. P., Chen, I. W., Dancheck, K. B., Krueger, J. A., Cooper, C. M., and Vacca, J. P. (1998) Design and synthesis of a series of potent and orally bioavailable noncovalent thrombin inhibitors that utilize nonbasic groups in the P1 position, *J. Med. Chem.* 41, 3210–3219.
24. Stubbs, M. T., Reyda, S., Dullweber, F., Moller, M., Klebe, G., Dorsch, D., Mederski, W. W., and Wurziger, H. (2002) pH-dependent binding modes observed in trypsin crystals: lessons for structure-based drug design, *ChemBioChem* 3, 246–249.
25. Katz, B. A., Sprengeler, P. A., Luong, C., Verner, E., Elrod, K., Kirtley, M., Janc, J., Spencer, J. R., Breitenbucher, J. G., Hui, H., McGee, D., Allen, D., Martelli, A., and Mackman, R. L. (2001) Engineering inhibitors highly selective for the S1 sites of Ser190 trypsin-like serine protease drug targets, *Chem. Biol.* 8, 1107–1121.
26. Mackman, R. L., Katz, B. A., Breitenbucher, J. G., Hui, H. C., Verner, E., Luong, C., Liu, L., and Sprengeler, P. A. (2001) Exploiting subsite S1 of trypsin-like serine proteases for selectivity: potent and selective inhibitors of urokinase-type plasminogen activator, *J. Med. Chem.* 44, 3856–3871.
27. Nienaber, V. L., Davidson, D., Edalji, R., Giranda, V. L., Klinghofer, V., Henkin, J., Magdalinos, P., Mantei, R., Merrick, S., Severin, J. M., Smith, R. A., Stewart, K., Walter, K., Wang, J., Wendt, M., Weitzberg, M., Zhao, X., and Rockway, T. (2000) Structure-directed discovery of potent non-peptidic inhibitors of human urokinase that access a novel binding subsite, *Struct. Folding Des.* 8, 553–563.
28. Stubbs, M. T., Huber, R., and Bode, W. (1995) Crystal structures of factor Xa specific inhibitors in complex with trypsin: structural grounds for inhibition of factor Xa and selectivity against thrombin, *FEBS Lett.* 375, 103–107.
29. Light, D. R., and Guilford, W. J. (2001) Discovery of the Factor Xa Inhibitor, ZK 807834 (CI-1031), *Curr. Top. Med. Chem.* 1, 121–136.
30. Wei, A., Alexander, R., Duke, J., Ross, H., Rosenfeld, S. A., and Chang, C.-H. (1998) Unexpected binding mode of tick anti-coagulant peptide complexed to bovine factor Xa, *J. Mol. Biol.* 283, 147–154.

BI0264061